Incident laser modulation of a repaired damage site with a rim in fused silica rear subsurface*

Li Li(李 莉)[a)†], Xiang Xia(向 霞)[a)], Zu Xiao-Tao(祖小涛)[a)], Yuan Xiao-Dong(袁晓东)[b)], He Shao-Bo(贺少勃)[b)], Jiang Xiao-Dong(蒋晓东)[b)], and Zheng Wan-Guo(郑万国)[b)]

[a)] *Institute of Physics and Electronics, University of Electronic Science and Technology of China, Chengdu* 610054, *China*
[b)] *Research Center of Laser Fusion, China Academy of Engineering Physics, Mianyang* 621900, *China*

(Received 23 July 2011; revised manuscript received 19 August 2011)

Local CO_2 laser treatment has proved to be an effective method to prevent the 351-nm laser-induced damage sites in a fused silica surface from exponentially growing, which is responsible for limiting the lifetime of optics in high fluence laser systems. However, the CO_2 laser induced ablation crater is often surrounded by a raised rim at the edge, which can also result in the intensification of transmitted ultraviolet light that may damage the downstream optics. In this work, the three-dimensional finite-difference time-domain method is developed to simulate the distribution of electrical field intensity in the vicinity of the CO_2 laser mitigated damage site located in the exit subsurface of fused silica. The simulated results show that the repaired damage sites with raised rims cause more notable modulation to the incident laser than those without rims. Specifically, we present a theoretical model of using dimpled patterning to control the rim structure around the edge of repaired damage sites to avoid damage to downstream optics. The calculated results accord well with previous experimental results and the underlying physical mechanism is analysed in detail.

Keywords: laser-induced damage, fused silica, mitigated damage site, three-dimensional finite-difference time-domain

PACS: 42.60.JF, 42.62.–b, 42.70.Ce, 46.15.–x **DOI:** 10.1088/1674-1056/21/4/044212

1. Introduction

Laser damage to optical components is a main issue for high power laser systems. Particularly for inertial confinement fusion (ICF) class lasers, the laser damage resistance of fused silica surfaces at 351 nm in the nanosecond range is of major concern.[1−5] The fused silica optics used as focusing elements in a high power laser system are generally quite thick and must be produced from high-quality, inclusion-free SiO_2, thereby making these elements relatively expensive and of high interest in terms of damage repair and recycling.[6] At present, as one of the most promising methods, a CO_2 laser operating at 10.6 μm has been reported to locally melt and evaporate the silica surface by producing typically smooth, Gaussian-shaped pits to avoid damage growth during consequent 351-nm laser irradiation.[7−12] In this way, the Si–O bonds are rebuilt and the stoichiometric ratio is recovered. The silica melt flows and so heals the subsurface small cracks. As a result, the damage resistance capability is improved. It is reported that two kinds of defects can be repaired by using a CO_2 laser.[7] One is the initial defect in the optics before laser irradiation and the other is the damage site created during irradiation.

Though CO_2 laser irradiation is a good method to raise the damage threshold, it also has some negative effects. After CO_2 laser irradiation, the fracture associated with damage can be removed by evaporation and re-melting. The resulting shape of repaired sites is always characterized by a crater region and a surrounding raised rim,[6,13] as shown in Fig. 1. The rim is formed from mass movement of silica at high temperatures from the low viscosity central region outwards, and can be several microns high for conditions used to mitigate surface damage.[6] Experimental investigations show that new damage always occurs in the surrounding area of the crater receiving CO_2 laser treatment, even when the surface is free from any other visible defects after 351-nm irradiation.[6,14] It is easy to understand that the outer rim of the repaired damage site can be regarded as a convex mirror and

*Project supported by the Fundamental Research Funds for the Central Universities (Grant No. ZYGX2010J045), the National Natural Science Fundation of China and the China Academy of Engineering Physics United Foundation (NSAF) (Grant No. 11076008), and the Foundation for Young Scholars of University of Electronic Science and Technology of China (Grant No. L08010401JX0806).

†Corresponding author. E-mail: jasmine2008@uestc.edu.cn

© 2012 Chinese Physical Society and IOP Publishing Ltd

the incident laser beam is focused as it passes through the repaired damage site. As a result, the electrical field is enhanced by the rim. This indicates that the control of the rim structure around the edge of typical mitigation sites is crucial to avoid damage growth. In order to alleviate the damage growth, Manyalibo *et al.*[6] presented 'dimpled' patterning formed in the rim region from an experiment standpoint.

Although the successful demonstration of the CO_2 laser operating method has motivated theoretical and experimental work to improve the process,[15–18] few studies have focused on the electrical field modulation investigation of the repaired damage sites.[19] In addition, there is no theoretical work discussing the effectiveness of the 'dimpled' patterning presented by Manyalibo and his coworkers. In the present work, a three-dimensional (3D) grid model of the repaired damage sites is built. The 3D finite-difference time-domain method is developed to solve the Maxwell equations. Then the electrical field intensity distribution in the vicinity of the repaired damage site in the rear subsurface of the fused silica is numerically simulated for the first time. The relationships between the maximal electrical field intensity in fused silica and the geometry of the repaired damage site are discussed. In addition, a 3D grid model of the dimpled-rim repaired damage site is constructed. Finally, calculations are employed to investigate the effect of the dimpling treatment on the modulation of the laser electrical field.

2. Models

Figure 1 shows the surface morphology of a typical repaired damage site in the exit surface of fused silica using an STIL contactless profilometer in corresponding ICF experiments.[6] The axial and lateral resolutions of the STIL profilometer were ~ 0.5 μm and ~ 1 μm, respectively, indicating that the damage site consists of two parts: the crater below the surface of fused silica, which satisfies a Gaussian distribution (Part 1); and the rim above the fused silica surface, which can be regarded as a Gaussian rotation (Part 2).

According to the experimental profile of the repaired damage site shown in Fig. 1, we built a 3D grid model of the damage site. In the model, the surfaces of the two parts, which are above and below the fused silica surface, respectively, can be described by the 3D equations

$$\begin{cases} z = z_{01} + A_1 \exp\left[\dfrac{-2}{w_1^2}((x-x_{01})^2 \right. \\ \qquad \left. + (y-y_{01})^2)\right] \quad \text{(Part 1)}, \\ z = z_{02} + A_2 \exp\left[\dfrac{-2}{w_2^2}(((x-x_{02})^2 \right. \\ \qquad \left. + (y-y_{20})^2)^{0.5} - d)^2\right] \quad \text{(Part 2)}, \end{cases}$$

where the xoy plane is parallel to the fused silica surface. (x_{01}, y_{01}, z_{01}) and (x_{02}, y_{02}, z_{02}) are the bottom positions of Part 1 and Part 2, respectively; d is a constant; A and W are the parameters controlling the repaired damage shape; A_1 and W_1 control the depth and the width of Part 1, respectively; A_2 and W_2 control the depth and the width of Part 2, respectively. Figure 2 shows the 2D schematic plot of the 3D grid model. The difference in grid size is $\delta = \lambda/12 = 29.25$ nm.

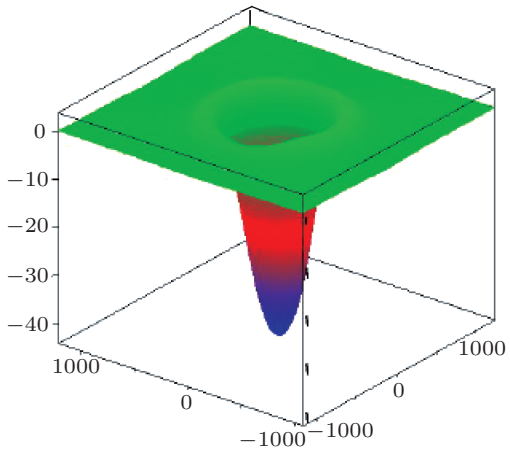


Fig. 1. (colour online) Surface morphology of the repaired site characterized by a crater region and a surrounding rim.[6]

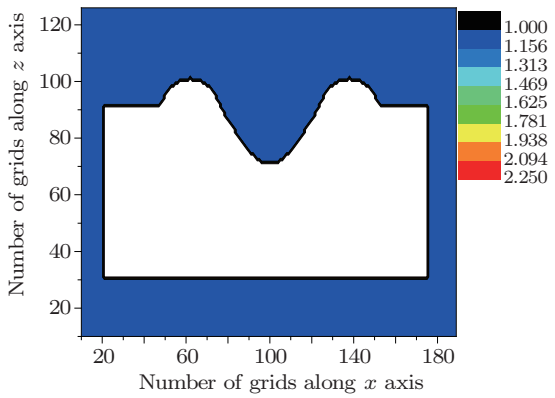


Fig. 2. (colour online) 2D schematic plot of the repaired crater with a raised rim.

3. Modulation to a 351-nm laser induced by the repaired damage site with a rim

During the numerical calculation, Maxwell's equations are solved by the 3D finite-difference time-domain method to calculate the electrical field intensity distribution in the vicinity of a repaired damage site.[18,19] The perfectly matched layer (PML) boundary condition is adopted.[19] The whole calculation domain is (180δ, 180δ, 126δ). The relative dielectric constant ε_r of fused silica is 2.25. The 351-nm laser with an amplitude 1.0 V/m travels in the direction normal to the surface, namely along the z axis. The TM wave is considered in this work. Other defects in the fused silica are ignored. It is assumed that the repaired damage site is in the exit surface and the crater is empty ($\varepsilon_r = 1.0$). The size of the damage site used for simulation is about 10 percent of the actual one due to the computer's capacity.

The modulation of the repaired damage site to the 351-nm laser is investigated. Firstly, the calculated electrical field distribution in the plane $y = 100\delta$ in the vicinity of a given repaired damage site is shown in Fig. 3. The parameters A_1, W_1, A_2, and W_2 are 40δ, 30δ, 10δ, and 20δ, respectively. In Fig. 3, the electrical field in fused silica is obviously scattered by the crater part and gathered by the rim part. The electrical field distribution in the plane $y = 100\delta$ in the vicinity of the given repaired damage site without the outer rim is shown in Fig. 4. A scattering region behind the damage site can be observed in both Fig. 3 and Fig. 4. Since the crater is empty (ε_r equals 1.0 which is less than that of fused silica), it looks like a concave mirror located at the position of the crater site. The incident laser is scattered by the concave mirror. So the scattering domain is created behind the repaired damage site. In addition, the maximum electrical field in Fig. 3 is greater than that in Fig. 4. In Fig. 3, the maximum electrical field appears just around the highest position of the rim. This is because the rim looks like a convex mirror located at the position of the outer rim of the damage site, as shown in Fig. 2. The converging effect of the convex mirror results in the electrical field enhancement in Fig. 3 is more remarkable than in Fig. 4 (without the converging effect of a rim).

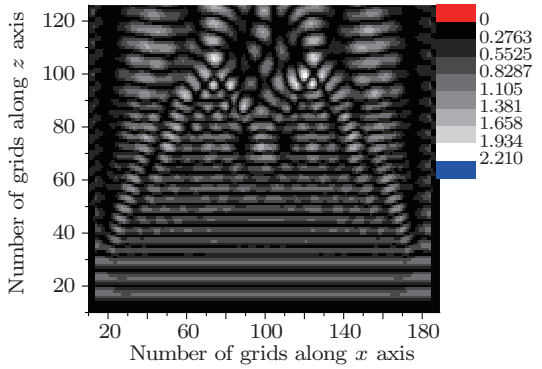


Fig. 3. (colour online) Distribution of electrical field at $y = 100\delta$ in the presence of a rim.

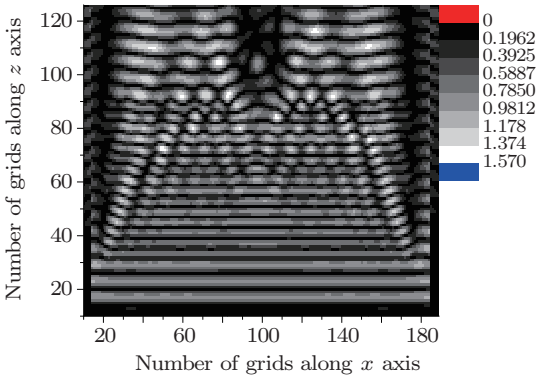


Fig. 4. (colour online) The distribution of electrical field at $y = 100\delta$ in the absence of a rim.

Secondly, we discuss the role that the repaired damage site geometry plays in the electrical field modulation, which is shown in Figs. 5 and 6. Figure 5 shows the effect of the geometry of the crater part of the repaired damage site on the electrical field modulation, where A_2 and W_2 are 10δ and 20δ, respectively. In Fig. 5(a), E_{max} first increases and then decreases with the increase of crater depth (the width $W_1 = 30\delta$ is given). It can be deduced that this phenomenon results from two factors. Firstly, as mentioned above, it looks like a concave mirror located at the position of the crater site. The incident laser is scattered by the concave mirror. Secondly, the scattering wave overlaps with the incident wave in fused silica. As they satisfy the interference reinforcing conditions in the overlap, the electrical field is enhanced.[19] However, as $A > 40\delta$, the scattering effect is more obvious because the crater becomes deeper. So E_{max} decreases. In Fig. 5(b) (given depth $A_1 = 40\delta$), E_{max} increases with crater width increasing, which is because the scattering effect becomes weaker with crack width increasing.

Figure 6 shows the correlation between the electrical field modulation and the height of the outer rim

part of the repaired damage site. The parameters A_1, W_1, and W_2 are 40δ, 40δ, and 10δ, respectively. It indicates that $E_{\max}$ increases with the increase of rim height. It is well known that the converging effect becomes stronger as the curvature of convex mirror becomes larger. In addition, the curvature of the rim, which can be regarded as a convex mirror, becomes larger as the height increases, so $E_{\max}$ increases with the increase of rim height.

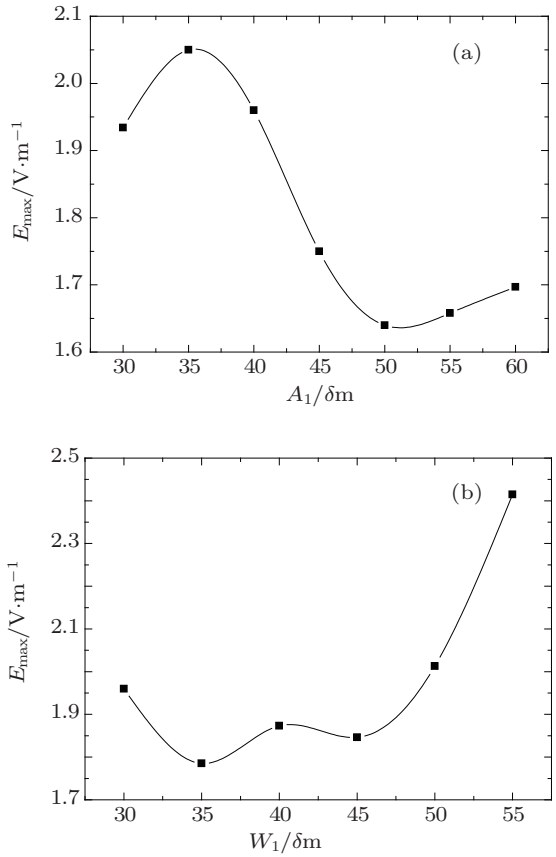


Fig. 5. Dependences of $E_{\max}$ on (a) crater depth and (b) crater width, respectively.

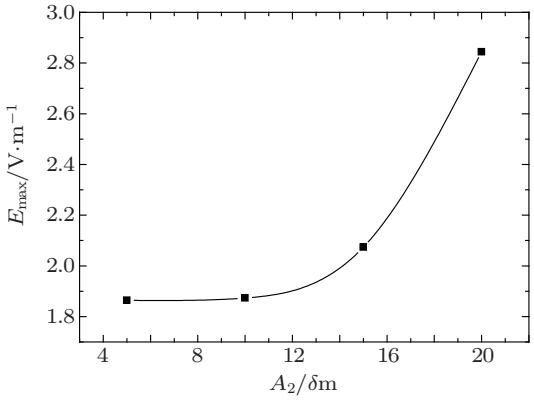


Fig. 6. $E_{\max}$ versus the height of rim.

4. Modulation mitigation of the dimpled rim

Figures 3–6 have proved that the modulation is notable by the rim around the repaired damage site. What can be done to mitigate the modulation of this kind of repaired damage to a 351-nm laser during the actual process? In 2007, Manyalibo *et al.*[6] presented an effective experimental solution to the control of the rim structure of repaired sites, i.e., the 'dimpled' patterning as given in Fig. 7. In order to investigate the modulation efficiency of this 'dimpled' patterning, a 3D grid model is constructed in this work. The 2D schematic plot of the 3D grid model is shown in Fig. 8.

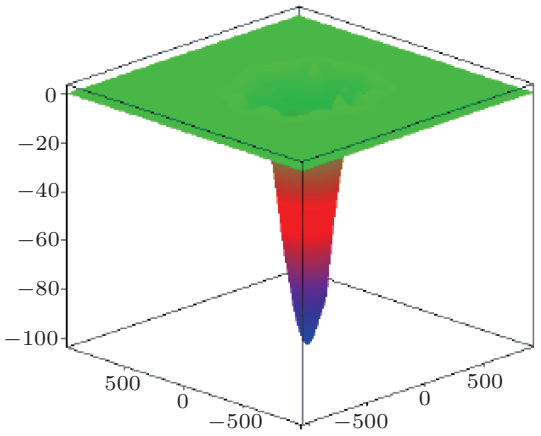


Fig. 7. (colour online) Surface morphology of the repaired site with a 'dimpled' pattern in the rim region.[6]

The electrical field distributions in the exit surface at $z = 100\delta$ for the damage site composed of a crater region and a surrounding rim are plotted in Fig. 9, where panel (a) corresponds to damage with a dimpled rim, and panel (b) with a non-dimpled rim. In Fig. 9, the parameters A_1, W_1, A_2, and W_2 are 30δ, 30δ, 10δ, and 20δ, respectively.

In Fig. 9, the electrical field enhancement regions can be observed in both panel (a) and panel (b) due to the convergence effect discussed in Section 3. The difference between panel (a) and panel (b) can be discussed from two aspects. On the one hand, the maximum electrical field in panel (b) (1.697 V/m) is 16.8% of $E_{\max}$ lower than that in panel (a) (2.039 V/m), which proves that the modulation of the repaired damage site with a dimpled rim is weaker than that without dimpled patterning. On the other hand, the distribution of the light enhancement positions is more random in panel (a), while the distribution of enhancement positions is nearly homocentric in panel (b). The

simulation results are well consistent with the experimental results presented in Ref. [6]. After dimpling treatment, the outer rim that looks like as a convex mirror is removed partially. The convergence effect of the rim becomes weak, which results in a lower maximum electrical field in panel (a) than in panel (b). The irregular rim shape (as shown in Fig. 8) is conducive to the random electrical field distribution (Fig. 9(a)). Therefore, the electrical field enhancement is indeed weakened after dimpling treatment.

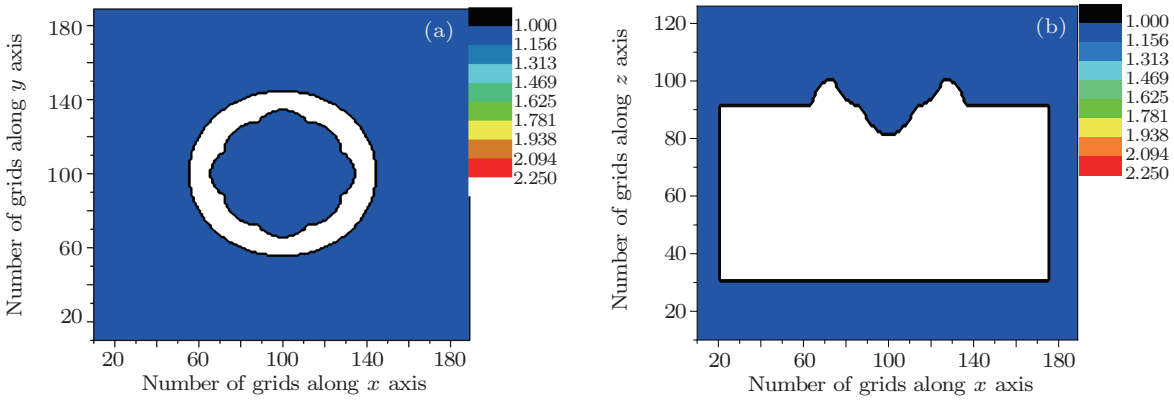


Fig. 8. (colour online) 2D schematic plot of the repaired pit with a 'dimpled' pattern in the rim region: (a) plan-view, (b) side-view.

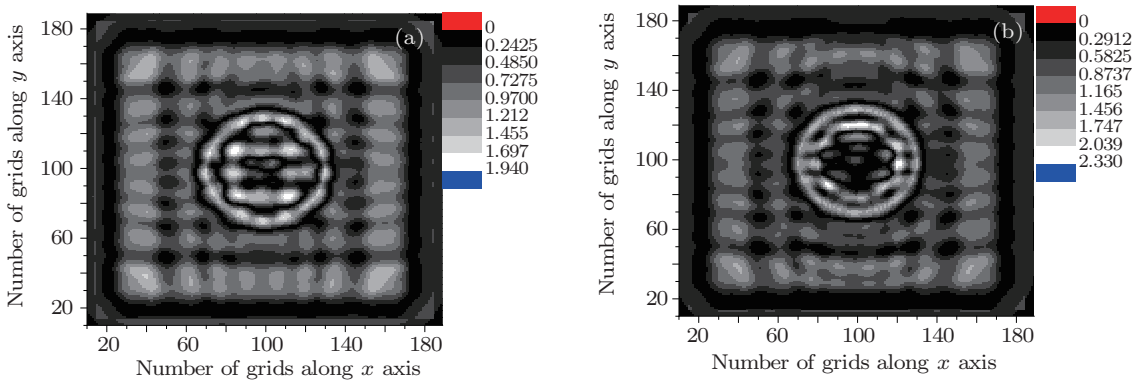


Fig. 9. (colour online) Distributions of electrical field in the exit surface at $z = 126\delta$ with a rim: (a) with a 'dimpled' rim and (b) with a non-dimpled rim.

5. Conclusion

The modulation to a 351-nm laser of the damage site with a rim repaired by a CO_2 laser is investigated theoretically in detail. Specially, the effectiveness of a dimpling treatment is discussed in this work. The conclusions are given as follows.

(i) The repaired site with an outer rim modulates the electrical field distinctly and the maximum enhancement appears around the highest position of the outer rim.

The modulation first increases and then decreases with the increase of crater depth of the damage site for a given width. In other words, a peak value of $E_{\max}$ appears with the increase of crater depth. The modulation becomes stronger with crater width increasing for a given crater depth. As for the rim, the modulation increases with the height increasing for a given width.

(ii) For the dimpled-rim sites, the intensification pattern is effectively dissipated to alleviate damage growth. The maximum electrical field (1.697 V/m) is much lower than that of the sites without dimpling treatment (2.039 V/m) in this work.

References

[1] Carr C W, Bude J D and Mange P De 2010 *Phys. Rev.* B **82** 184304

[2] Deng H X, Zu X T, Xiang X and Sun K 2010 *Phys Rev. Lett.* **105** 113603

[3] Chen X Q, Zu X T, Zheng W G, Jiang X D, Lu H B, Ren H, Zhang Y Z and Liu C M 2006 *Acta Phys. Sin.* **55** 1201 (in Chinese)

[4] Xiang X, Chen M, Chen M Y, Zu X T, Zhu S and Wang L M 2010 *Chin Phys.* B **19** 018107

[5] Deng H X, Xiang X, Sun K, Yuan X D, Jiang X D, Zheng W G, Gao F and Zu X T 2010 *Chin Phys.* B **19** 107801

[6] Manyalibo, Matthews J, Bass Isaac L and Gabriel Guss M 2007 *Proc. SPIE* **6720** 67200A

[7] Brusasco R M, Penetrante B M, Butler J A and Hrubesh L W 2002 *Proc. SPIE* **4679** 40

[8] Prasad R R, Bruere J R, Peterson J, Halpin J M, Lucero P, Mills S, Bernacil M and Hackel R 2004 *Proc. SPIE* **5273** 288

[9] Prasad R R, Bruere J R, Halpin J, Lucero P, Mills S, Bernacil M and Hackel R P 2004 *Proc. SPIE* **5273** 296

[10] Bass I L, Guss G M and Hackel R P 2005 *Proc. SPIE* **5991** 59910C

[11] Guss G, Bass I, Draggoo V, Hackel R, Payne S, Lancaster M and Mark P 2006 *Proc. SPIE* **6403** 64030M

[12] Mendez E, Nowak K M, Baker H J, Villarreal F J and Hall D R 2006 *Appl. Opt.* **45** 5358

[13] Xiang X, Zheng W G, Yuan X D, Dai W, Jiang Y, Li X B, Wang H J, Lü H B and Zu X D 2011 *Chin. Phys.* B **20** 044208

[14] Gallais L, Cormont P and Rullier J L 2009 *Proc. SPIE* **7504** 75040Z

[15] Palmier S, Gallais L, Commandré M, Cormont P, Courchinoux P, Lamaignère L, Rullier J L and Legros P 2009 *Appl. Surf. Sci.* **255** 5532

[16] Guss G, Bass I, Hackel R and Demos S 2008 *Appl. Opt.* **47** 4569

[17] Bertussi B, Cormont P, Palmier S, Legros P and Rullier J L 2009 *Opt. Express* **17** 11469

[18] Stevens-Kalceff M C and Wong J 2005 *J. Appl. Phys.* **97** 113519

[19] Li L, Xiang X, Zu X T, Wang H J, Yuan X D, Jiang X D, Zheng W G and Dai W 2011 *Chin. Phys.* B **20** 074209